Surface-Enhanced Infrared Ellipsometry of Self-Assembled Undecanethiol and Dodecanethiol Monolayers on Disordered Gold Nanoisland Substrates

D. C. Bradford,[†,‡] E. Hutter,[†] J. H. Fendler,*[,†] and D. Roy*[,‡]

Center for Advanced Materials Processing and Department of Physics, Clarkson University, Potsdam, New York 13699

Received: May 25, 2005; In Final Form: August 31, 2005

Infrared spectroscopic ellipsometry (IRSE) is a powerful optical probe of various chemical and physical properties of molecules adsorbed onto solid surfaces. In particular, IRSE can be useful for detecting adsorption-induced changes in the IR spectra of self-assembled monolayers (SAMs), and unlike traditional IR absorption spectroscopies, IRSE provides useful information about the phase of the reflected radiation from the SAMs. However, in the standard IRSE experimental geometry using flat substrates for SAMs, the detectable signal containing these phase data is considerably weaker than the corresponding absorbance data. In our present work, we demonstrate that enhancing the local optical fields at the sample surface through the use of a disordered Au nanoisland substrate can substantially increase both these absorbance and phase signals. We also demonstrate how this surface-enhanced infrared spectroscopic ellipsometry (SEIRSE) can be utilized for straightforward analysis of absorption peak widths, as well as to obtain information about the orientation of the terminal methyl on adsorbed SAMs. As model SAMs for this study, we use undecanethiol (UDT) containing 10 CH_2 units and a terminal CH_3 group, as well as dodecanethiol (DDT) containing 11 CH_2 units with its terminal CH_3 at a different orientation than UDT. We show that surface-enhanced IRSE is sensitive to subtle vibrational signatures of the differently oriented terminal methyls of these two homologous alkanethiol SAMs.

1. Introduction

Infrared spectroscopic ellipsometry, IRSE, has been shown to be a valuable technique for the characterization of ultrathin films and self-assembled monolayers (SAMs).[1−7] Specifically, while the thickness and the complex refractive index of the adsorbed film or SAMs can be readily determined by traditional ellipsometry in the visible range of the spectrum, functional-group accessibility, and hence information on the spatial orientation of these groups, only becomes available through the utilization of IRSE. In fact, the most significant benefit of IRSE is that it measures *both* absorbances and phase parameters in the IR region of the spectrum. In a recent publication, we reported the effects of thickness and morphology of gold substrates on the IRSE signal of an octadecylmercaptan (ODM) SAM.[8] In that work, similar spectral features were observed on 23.0 and 100.0 nm thick continuous gold substrates, but different features as well as surface enhancements were observed by using 22 nm thick gold nanoislands as substrates. In the present work, we extend these studies to further the utilization of the phase information obtained in IRSE. To boost the relatively weak phase signal of a SAM, we employed gold nanoisland substrates for surface-enhanced infrared ellipsometry, SEIRSE. Although surface-enhanced infrared reflection absorption spectroscopy, SEIRRAS, is well recognized,[9−12] to the best of our knowledge no previous work has been reported on SEIRSE. Two homologous alkanethiol SAMs, undecanethiol (UDT, 11 carbon atoms) and dodecanethiol (DDT, 12 carbon atoms), are selected as model samples for our present study. These two SAMs are of comparable lengths and hence are expected to orient and pack in comparable ways on the substrate. At the same time, the two molecules having different (odd and even) numbers of carbon atoms should exhibit the so-called "odd−even" effect[13,14] due to the changed orientation of the terminal methyl group in the two cases. Thus, UDT and DDT are ideally suited for checking the sensitivity of the enhanced ellipsometric data to the different terminal methyl orientations. We show here that these subtle orientation effects remain undetected in the relatively weak IRSE signal but are clearly manifested in the enhanced phase data in SEIRSE. Surface enhancement is highly sensitive to the substrate morphology. We use internal normalization and compare absorption modes where the transitional dipole moments are known to experience the same electric fields. Using the phase information extracted from these SEIRSE data, we also obtain absorption strength and band maxima in good resolution and without the need for determining the baseline for the convoluted absorption data.

2. Background

Surface Enhanced Infrared Spectroscopic Ellipsometry (SEIRSE). Let us briefly note the main useful features of SEIRSE and discuss the optical parameters that can be measured using this technique.[1−14] For this discussion, we consider a simple four-phase sample configuration, denoted as (1234), in the external reflection geometry. In this arrangement, a disordered Au nanoisland film (phase 2) is vacuum deposited onto ZnSe (phase 1) and the sample SAM (phase 3) is adsorbed onto the disordered Au nanoisland substrate. A reflected probe IR light beam of polarization state γ (with $\gamma \equiv$ s or p) is detected in phase 4 (air in the present work). The "reference" system not containing the SAM phase 3 is denoted as (124). The complex Fresnel reflection factors for the sample (1234) and the reference (124) systems are expressed as $r^{\gamma}_{1234} = |r^{\gamma}_{1234}| \exp(i\delta^{\gamma}_{1234})$ and $r^{\gamma}_{124} = |r^{\gamma}_{124}| \exp(i\delta^{\gamma}_{124})$, where δ^{γ}_{1234} and δ^{γ}_{124}

* To whom correspondence should be addressed. E-mail: fendler@clarkson.edu. Tel: (315) 268 7113. Fax: (315) 268−4416. E-mail: samoy@clarkson.edu. Tel: (315) 268 6676. Fax: (315) 268−6610.

[†] Center for Advanced Materials Processing, Box 5814.

[‡] Department of Physics, Box 5820.

10.1021/jp052764c CCC: $30.25
Published on Web 10/15/2005

are the effective phase angles for the (1234) and (124) systems, respectively. In IRSE, one measures two sets of optical parameters (namely, the ellipsometric parameters), ψ_{1234} (polarization ratio) and Δ_{1234} (phase retardation) for the (1234) system, along with the corresponding ψ_{124} and Δ_{124} for the (124) system. The ellipsometric variables are related to the Fresnel factors:[1−16] $\psi_{1234} = \tan^{-1}[|r^{p}_{1234}|/|r^{s}_{1234}|]$, $\psi_{124} = \tan^{-1}[|r^{p}_{124}|/|r^{s}_{124}|]$, $\Delta_{1234} = \delta^{p}_{1234} - \delta^{s}_{1234}$, and $\Delta_{124} = \delta^{p}_{124} - \delta^{s}_{124}$, where the ψ and Δ parameters are interdependent through the Kramers−Kronig relation. The reflectances for these sample and reference systems are written as $R^{\gamma}_{1234} = |r^{\gamma}_{1234}|^2$ and $R^{\gamma}_{124} = |r^{\gamma}_{124}|^2$, respectively. The IR absorbance (A^{γ}) of the SAM, measured with γ-polarized radiation in the external reflection, has the form: $A^{\gamma} = \ln(R^{\gamma}_{1234}/R^{\gamma}_{124})$. It is this absorbance parameter that is available through traditional IRRAS measurements. The main advantage of IRSE over IRRAS is that IRSE provides information about the phases of the Fresnel coefficients in addition to measuring A^{γ} (associated with the moduli of the Fresnel reflection coefficients). This phase information is useful for analyzing the overall (molecular chain) orientation of adsorbed molecules[16−18] and, as we demonstrate later in this paper, can also be utilized to readily determine certain parameters (such as integrated area and width) of absorption peaks that would otherwise require complex deconvolution procedures. In addition, it will be shown in our present work that IRSE, along with the surface selection rule of metallic substrates, has the potential of probing specific information about the orientation of terminal groups of adsorbed molecules on Au. To utilize these capabilities of IRSE, we use the framework of differential ellipsometry to analyze the optical data. In this approach, a complex optical density function D is defined as $D = (D_p - D_s) = (\mathrm{Re}D + j\mathrm{Im}D)$, where $j = (-1)^{1/2}$, with ReD and ImD representing the real and imaginary parts of D, respectively[8]

$$\mathrm{Re}D \equiv \frac{1}{2}(A^{p} - A^{s}) = \ln\left[\frac{\tan(\psi_{123})}{\tan(\psi_{1234})}\right] \quad (1)$$

$$\mathrm{Im}D = (\Delta_{124} - \Delta_{1234}) \quad (2)$$

The terms ψ_{124}, ψ_{1234}, Δ_{124}, and Δ_{1234} are experimentally measured in IRSE in the spectral region where the predominant vibrations of the sample SAM are expected.[19] Subsequently, the IR spectra of ReD and ImD are determined by using eqs 1 and 2. If the experimental conditions are favorable to support the surface selection rule ($R^{s}_{1234} \approx R^{s}_{124}$) for IR absorption,[20−23] then ReD represents the (p-polarized) absorption spectrum, $A_p \cong 2(\mathrm{Re}D)$.

As we have shown in our previous work (and will be further demonstrated in the present report), the signal levels of the ImD spectra are in general considerably weaker than those corresponding to the ReD spectra and consequently, it can be difficult to obtain useful information from it. This problem can be remedied by incorporating SEIRRAS in the framework of IRSE. In this approach, the disordered gold nanoislands used for supporting the SAM enhance the optical fields, and hence the infrared absorption signal, by localized surface plasmon resonance. Detailed theoretical considerations for this effect have been discussed by other authors[9,10,23] and will not be included in our report. Previously, this substrate roughness induced enhancement has been used in IRRAS but, to our knowledge, has not been systematically integrated with IRSE. In our previous work, we have shown that enhanced optical absorption could also be utilized in IRSE, and this approach will be used in our present study of SEIRSE.

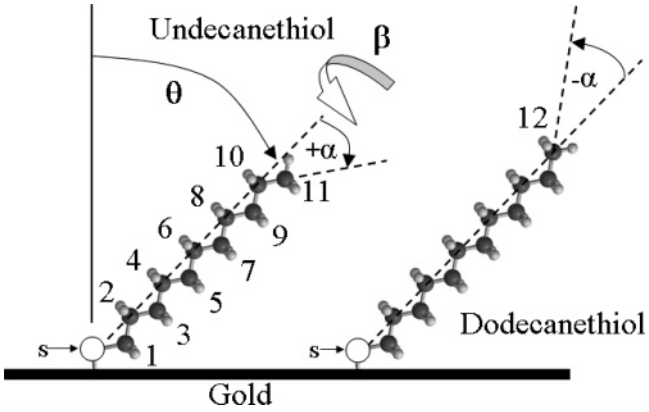

Figure 1. Schematic diagram showing space filling models of UDT and DDT chemisorbed on a gold substrate. The numbers of the carbon atoms in each SAM are labeled, and the different angles associated with molecular orientation are indicated. θ is the tilt angle of the molecular axis relative to the surface normal, α is the additional tilt of the terminal C−C bond, and β is the rotation angle of the trans-carbon backbone around its molecular axis. The condition $\beta = 0°$ puts all the carbons in the perpendicular plane defined by the surface normal and the molecular axis.

Model SAMS. Molecules of *n*-alkanethiols are known to attach to gold surfaces by chemisorption to form close-packed SAMs. Two such SAMs, UDT and DDT, chosen for the present work, are schematically shown in Figure 1 using space filling models. According to an authoritative recent review,[24] both these SAMs are expected to have adsorption configurations with fully extended chains in a nearly all-trans configuration. The tilt angle θ (typically around 30°) with respect to the substrate surface is determined by the optimization of the van der Waals contact in the assembly and is the same for both UDT and DDT on Au. The twist angle β is measured between the plane of the CCC bond and the plane containing the surface normal and the hydrocarbon chain ($0° \le \beta \le 90°$, positive for counterclockwise rotation). The value for β was determined[13] to be 52−55 by fitting IRRAS spectra to theoretical models for C_{16}−C_{20} alkanethiol SAMs on Au(111) substrates. The methyl tilt angle α describes the orientation of the C−CH_3 bond with respect to the molecular axis. The sign of this α is negative or positive depending on whether the SAM contains an even or odd number of carbon atoms (that is, an odd or even number of CH_2 groups), respectively. Thus, α is positive for UDT (having an odd number of C atoms) and negative for DDT (having an even number of C atoms), although the magnitude of α is the same (35.3°) for both these SAMs.[13,24,25] These different signs of α for the two SAMs are expected to result in the so-called "odd−even effect" that is often observed in IR absorption studies of alkyl chains in the *all-trans* conformation on Au.[13] This effect is generally manifested in an odd−even modulation of the vibrational signals of the methyl modes;[13,24−27] for SAMs containing an odd number of carbon atoms (even number of CH_2 groups), the absorption intensity of the CH_3 symmetric mode is lower than that of the corresponding asymmetric CH_3 mode, and the situation is reversed for SAMs containing an even number of carbon atoms, owing to the orthogonality of the modes and the sensitivity to the surface normal components of the technique. IR absorption data that contain this odd−even effect can be particularly useful for quantitative analyses of both the overall (θ) and local (α and β) orientations of SAMs adsorbed on Au. Our main reason for choosing UDT and DDT (odd- and even-carbon SAMs) here is to examine the sensitivity of SEIRSE in detecting this odd−even effect.

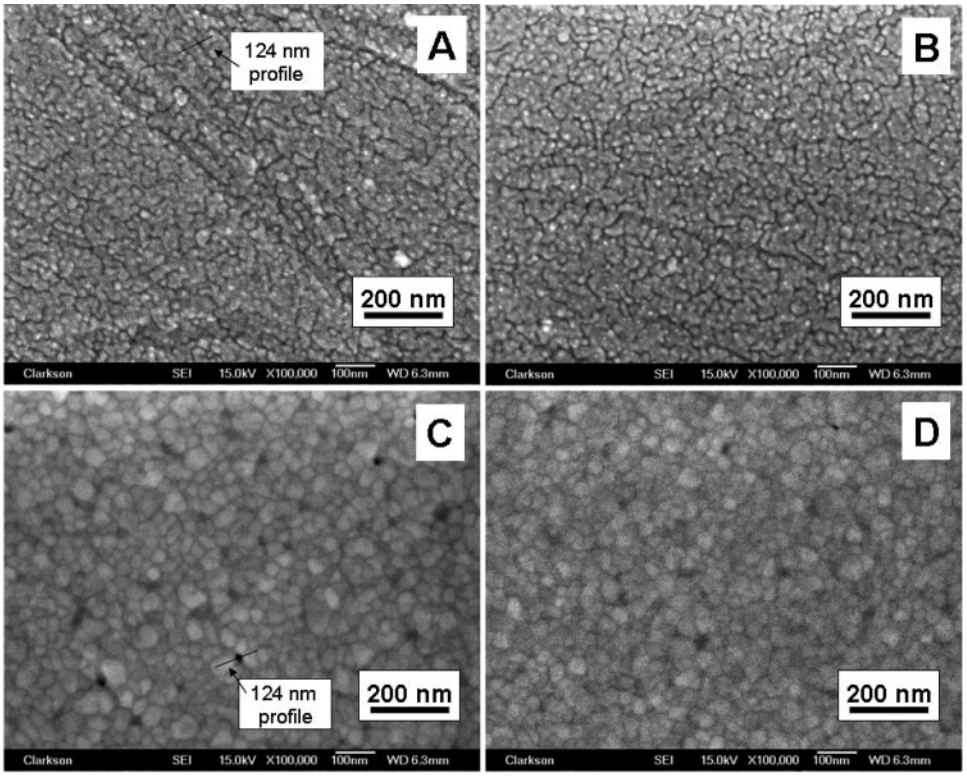

Figure 2. (A) SEM image of 20 nm thick disordered gold nanoislands (under a monolayer of self-assembled UDT). (B) SEM image of 20 nm thick disordered gold nanoislands (under a monolayer of self-assembled DDT). (C) SEM image of 188 nm thick gold film grown on 1.6 nm thick chromium (under a monolayer of self-assembled UDT). (D) SEM image of a different portion of C (under a monolayer of self-assembled DDT). The lines drawn in A and C show the profiles used for the estimation of surface roughness.

3. Experimental Section

The experimental instruments and procedures used in this work have been described in detail in our earlier papers.[8,20] In brief, gold was deposited onto two clean ZnSe hemispheres simultaneously in an Edwards AUTO306 vacuum deposition chamber (7.0×10^{-6}–1.0×10^{-5} Torr and at a deposition rate of 8.0×10^{-3} nm/s), producing Au nanoislands. The two thick gold substrates were deposited onto two halves of a BK7 glass slide (precoated by 1.6 nm thick chromium) under 4.0×10^{-6} Torr at a deposition rate of 0.39 nm/s. The thickness and deposition rate of the films were monitored with a quartz crystal microbalance at a natural resonance frequency of 6 MHz. The gold nanoisland films were kept under vacuum until the background data was collected the next day. The thick gold substrates were treated with piranha solution just prior to their use. The thicknesses of the deposited SAMs on Au were determined by using the surface plasmon resonance (SPR) technique as described in detail in our previous reports.[1,28] All gold nanoisland substrates were thoroughly cleaned with water and ethanol and then were immersed in 1 mM ethanolic solutions of UDT or DDT for 1 h, followed by thorough washing by water and ethanol and drying by nitrogen. All data sets needed for the determination of the optical density function D for both samples were completed within three days, with the samples kept in a vacuum desiccator when not being probed. A JEOL JSM-7400F SEM was used to obtain images of the Au substrates. The image analysis software ImageJ was used to estimate the surface roughness of the Au substrates.

IRSE data were recorded with a Digilab FTS 7000 spectrometer in rapid scan mode at 20 kHz, using an undersampling ratio of 2, and co-adding 512 scans staggered as four groups of 128 scans cycling between three polarization analyzer directions. The experimental uncertainty in the stepping motor/gears was (quoted by the manufacturer) $\pm 0.2°$. A gold grid polarizer was used to obtain linearly polarized incident radiation, set at 45° to the plane of incidence with an angle of incidence of 70°. A second motorized gold grid polarizer, located between the sample and a liquid nitrogen cooled narrow band HgCdTe (MCT) detector, selected between 0° (or 180°, p), 90° (or 270°, s), and −45° (or 135°, −45). These data were processed following the procedure described in our earlier work (eq 12 in ref 8) to obtain the ellipsometric parameters, Δ and ψ. Subsequently, these parameters were converted to the optical density functions using eqs 1 and 2.

The convention used for rotations of the electric field vector relative to the plane of incidence was positive for counterclockwise rotations looking in the direction of the propagation vector. A 90° rotation of the analyzer relative to the incident beam produced the largest of the three signals as expected for the near grazing angle reflections from metallic substrates. The aperture width (2 cm), resolution (4 cm^{-1}), and sensitivity (1) were kept fixed in all experiments. The sampling regimen was designed to average out both random error and systematic errors due to minute changes in the beam, ambient environment (temperature, relative humidity, etc.), and detector sensitivity. After an initial 30 min purge of the FTS 7000 and external experimental chamber, it took an average of ~20 min to obtain data for the ellipsometric parameters Δ and ψ while continually purging with a Parker Balston purge gas generator.

4. Results and Discussion

Surface Morphologies of Disordered Gold Nanoislands. SEM images of 20 nm thick disordered gold nanoislands (under SAMs) and 188 nm thick continuous gold films are illustrated in Figure 2. Using the ImageJ image analysis program, we determined 5% and 11% dark cracks in images A and B,

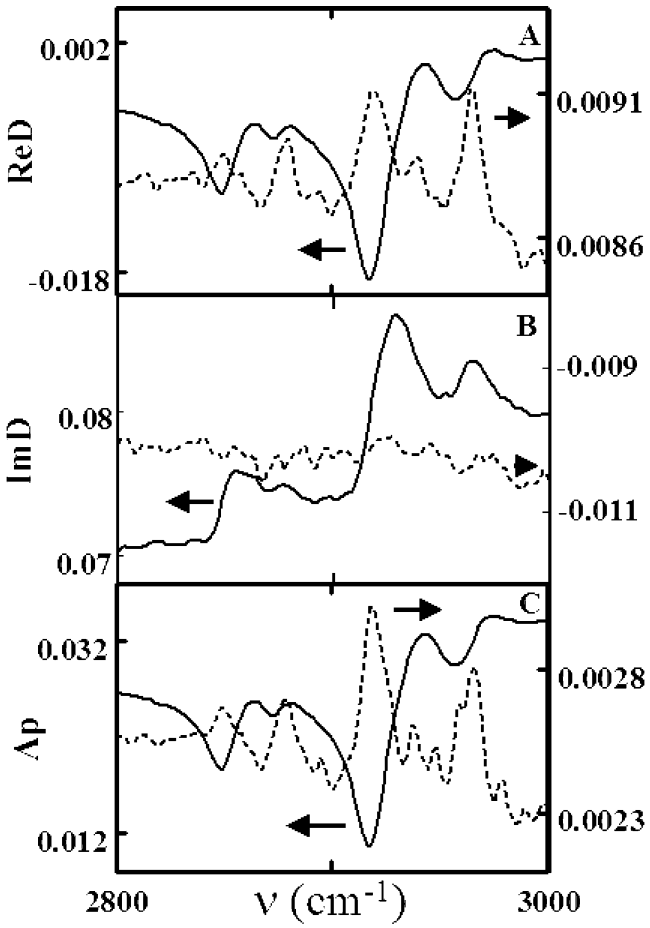

Figure 3. Plots of Re*D*, Im*D*, and A_p (in panels A, B, and C, respectively) against wavenumbers (ν) for UDT on disordered gold nanoislands (solid line, scale on the left) and on a 188 nm thick gold film (dashed line, scale on the right).

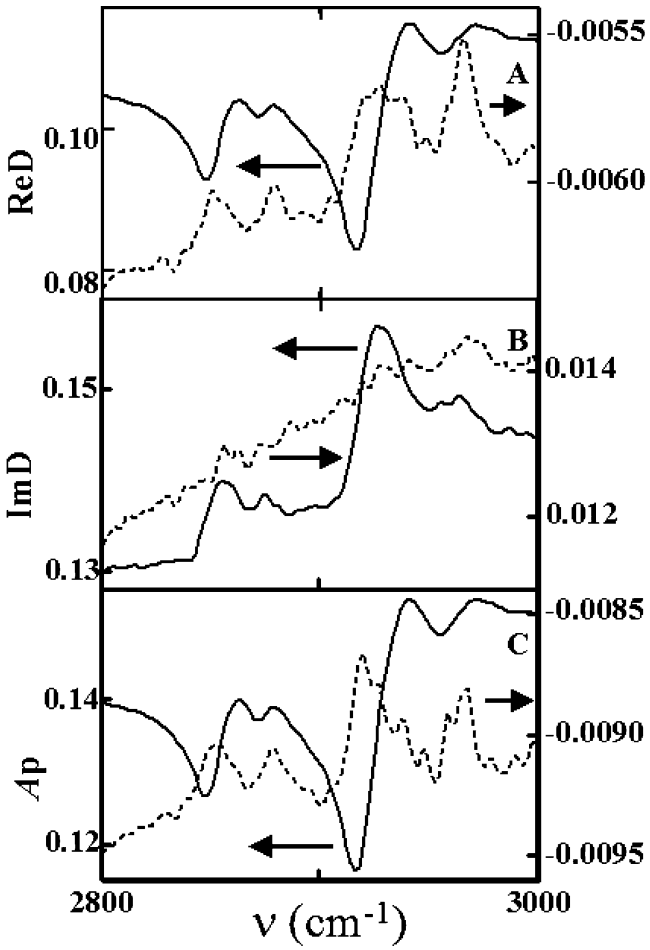

Figure 4. Plots of Re*D*, Im*D*, and A_p (in panels A, B and C, respectively) against wavenumbers for DDT on disordered gold nanoislands (solid line, scale on the left) and on a 188 nm thick gold film (dashed line, scale on the right).

respectively. The morphologies seen in A and B in Figure 2 are quite similar to those reported previously by us[8] and others.[29−31] It appears that the rather large and relatively flat areas between the cracks in the disordered gold nanoislands are comparable to the flat terraces on the continuous films. The lines on images A and C indicate where profiles of the gray scale were drawn in an attempt to quantify the surface roughness. Assuming the SEM image gray scale is linearly proportional to height, and the cracks in A and the pit in C extend the full nominal width of the gold, a bracket of ±9.5 nm encompasses the variation in the nanoisland terrace, whereas a bracket of ±35 nm is needed to encompass the roughness of the thick gold terrace. There was great variability between different profiles. Annealing can smooth out Au(111) films down to the nm scale, but we had not annealed the continuous gold films since our goal was to make use of surface enhancements by disordered gold nanoisland substrates.[9,10] The resistivities measured for the disordered gold nanoisland substrates (2.87×10^{-5} and 3.18×10^{-5} Ω cm) were found to be quite similar to those we reported previously (1.88×10^{-5} Ω cm).[8] In contrast, the resistivity of the 188 nm thick gold film, 4.4×10^{-6} Ω cm, is quite comparable to that of bulk gold (2.35×10^{-6} Ω cm).

Surface Enhancement of Infrared Ellipsometry Spectra. In Figure 3 we compare the (A) Re*D*, (B) Im*D*, and (C) A_p spectra for UDT adsorbed on Au films, using the experimentally obtained results for IRSE (dashed lines) and SEIRSE (solid lines). The corresponding results for DDT are shown in Figure 4. The spectral region (plotted against wavenumber, ν) of interest for the given SAMs is in the 2800−3000 cm^{-1} region, where all the major vibrational features of UDT and DDT are located. These vibrational modes are summarized and compared with literature values[13,32] in Table 1. The d^+ mode represents an in-plane (ip), symmetric (sym) CH_2 stretching vibration. Fermi resonance splitting of this in-plane, symmetric CH_2 stretch (expected in the 2895−2907 cm^{-1} region[13]) is not resolved in the present data. The r^+ mode is associated with the symmetric CH_3 methyl stretch. Fermi resonance between r^+ and CH_3 bending is also known to result in a band around 2935 cm^{-1} (r_{FR}^+),[25] but again, this specific band is not resolved in our data. The in-plane and out-of-plane asymmetric vibrations of CH_3 are indicated as r_a^- and r_b^-, respectively. CH_2 asymmetric (asym) stretching is indicated by the d^- mode. The observed absorption by the CH_2 asymmetric modes means that the plane of the trans-carbon backbone must be rotated out of the surface normal plane defined by the angle β in Figure 1.

The disordered gold nanoisland substrates in Figures 3 and 4 are seen to enhance both the Re*D* and Im*D* signals approximately 40-fold. The mechanism of this enhancement originates from the optical excitation of localized surface plasmons within the metallic nanoisland structures of the rough Au substrate, and this effect has been described in detail in previous publications.[1,8] Despite its enhanced signal, the SEIRSE signal in Figures 3 and 4 loses some resolution; the CH_3 sym Fermi resonance component (2939 cm^{-1}) is the most obvious additional stretching mode resolved only on the continuous gold substrates. The vibrational modes of both SAMs used here

TABLE 1: Description of Vibrational Modes of UDT and DDT Detected Using IRSE and SEIRSE

mode[a] (notation)	SAM	Re*D* in IRSE[b] (cm^{-1})	Im*D* in IRSE[e] (cm^{-1})	Re*D* in SEIRSE [f] (cm^{-1})	Im*D* in SEIRSE[g] (cm^{-1})	literature values[h] (cm^{-1})
CH_2 sym	UDT	2850	unresolved	2849	2847	2850, 2853
(d^+)	DDT	2850	unresolved	2849	2849	
CH_3 sym	UDT	2879	unresolved	2872	2876	2879
(r^+)	DDT	2879	unresolved	2872	2874	
CH_2 asym	UDT	2919	unresolved	2918	2914	2918, 2925[i],
(d^-)	DDT	2927	unresolved	2916	2914	2935[j]
CH_3 asym	UDT	2939[c], 2966[d]	unresolved	2957	2951[c], 2960[d]	2954[c], 2964[d]
(r_a^- or r_b^-)	DDT	2949[c], 2966[d]	unresolved	2955	2954[c], 2962[d]	

[a] Abbreviations: sym = symmetric, asym = symmetric, ip = in-plane, op = out-of-plane. [b] Peak frequencies, obtained from Figure 5A. [c] Out-of-plane (r_b^-). [d] In-plane (r_a^-). [e] Data refer to Figure 5A. [f] Peak frequencies, obtained from Figure 6. [g] Midpoint frequencies between (fwhm) extremum points in Figure 6. [h] Reference 13 and references therein. [i] Terminal CH_2S. [j] CH_3 Fermi resonance (r_{FR}^+).

should experience comparable electromagnetic enhancement. The addition of a CH_2 unit, to go from UDT to DDT, may slightly increase the absorption of the CH_2 stretching modes but not the relative intensities of the mutually orthogonal asymmetric and symmetric modes due to their symmetry about the molecular axis. Moreover, because the overall vibrational features of the SAMs are comparable in the IRSE (continuous Au substrate) and SEIRSE (Au nanoislands) measurements, the two Au substrates used in these experiments most probably provide similar tilt angles irrespective of the detailed substrate morphologies.

The thicknesses of UDT and DDT obtained (using SPR) on a 122 nm thick continuous Au film were found to be 10.80 and 11.16 Å for UDT and DDT, respectively. By the use of the terminal hydrogen to terminal hydrogen linear lengths of 15.70 Å (UDT) and 16.94 Å (DDT), the above film thicknesses yield the tilt angles (θ) of 46.5° and 48.8° for UDT and DDT on the continuous (flat) Au substrate, respectively. As we noted above, it is likely that the respective orientations of UDT and DDT on the rough Au substrate used here are comparable to the aforementioned values of θ. The general agreement between Re*D* and A_p spectra (panels A and C in Figures 3 and 4) observed for both UDT and DDT SAMs on both continuous and disordered gold nanoisland substrates confirms the applicability of the surface selection rule mentioned in the context of eq 2; this agreement is even better for surface-enhanced signals.

The observation that the rough Au substrates actually support the surface selection rule implies that the value of θ on the rough Au surface is probably not different from that on the continuous flat substrate. We note in this context that the low-frequency CH_2 wagging mode progression region of alkanethiols usually contains useful information about chain conformation and orientation.[13,24] However, in our present SEIRSE measurements, this low-frequency region is not properly resolved beyond the background features of the substrate and impurities. Therefore, to discuss the implications of our SERIRSE data, we focus primarily on the high-frequency C−H region.

A prominent characteristic feature of the SEIRSE data in Figures 3 and 4 is that the enhanced Re*D* (and hence the corresponding A_p) spectra appear "inverted" with respect to their corresponding unenhanced spectra obtained with IRSE. This specific effect has been previously reported by other authors[33−35] as well as by us[8] and is generally associated with changes in the complex dielectric function of the SAM-supporting substrate in going from the flat to the rough Au substrate.[35] The dielectric function ϵ_{Au}^{eff} of the rough Au surface contains contributions of both Au nanoisland structures and the surrounding media (adsorbed SAM and air in this case)—as described in the commonly used effective medium approximations. The simple dielectric function ϵ_{Au} of the flat Au film generally has quite different values for both its real and its imaginary components in comparison with those of ϵ_{Au}^{eff}. The dielectric functions of the flat and rough Au films are included in the Fresnel coefficients for both the 124 and 1234 multiphase systems involving the corresponding substrate films. These formulas are different for s- and p-polarized lights; as a result, the strengths of the roughness-induced changes in the Fresnel coefficients of the SAM-supporting Au film can be different for the two polarization states of the probe light. The Re*D* for the four-phase experimental sample using a flat Au film in layer 2 has the form: $ReD = \ln[|\rho_{124}|/|\rho_{1234}|]$, where the complex polarization ratios are defined as $\rho_{1234} = (r^p_{1234}/r^s_{1234})$ and $\rho_{124} = (r^p_{124}/r^s_{124})$. As we switch to the four-phase system containing a rough Au film, the dielectric function of phase 2, $\epsilon_2 = \epsilon_{Au}$ (defining $|\rho_{1234}|$ and $|\rho_{124}|$) changes to $\epsilon_2 = \epsilon_{Au}^{eff}$, which leads to the new polarization ratio amplitudes, $|\rho'_{124}|$ and $|\rho'_{1234}|$. In the latter case, *D* changes to a new value *D′*, which is now obtained by replacing $|\rho_{124}|$and $|\rho_{1234}|$ by their corresponding primed quantities.[8] Under this condition, and depending on the detailed relationship between the terms ($|\rho'_{1234}|/|\rho'_{124}|$) and ($|\rho_{1234}|/|\rho_{124}|$), it is possible to have a spectrum for Re*D′* that would appear as Re*D′* ≈ *a*(1-Re*D*), with *a* being a constant. This peak inversion effect is elaborated using experimental data in Figure 5, where the uninverted, unenhanced Re*D* spectra in panel A for UDT (solid line) and DDT (dashed line), obtained with IRSE, are compared with the corresponding enhanced spectra of the parameter (1-Re*D*) in panel B, with Re*D* taken from the SEIRSE data of Figures 3A and 4A. In other words, the solid and dashed line plots in Figure 5A represent the dashed line plots of Figures 3A and 4A, respectively. The molecular absorption features in the surface-enhanced (1-Re*D*) graphs of Figure 5B exhibit the same structures of their corresponding features observed in the unenhanced Re*D* graphs of Figure 5A. In addition, the main absorption peaks in Figure 5B are noticeably well defined and appear considerably above the background noise level. Thus, according to the above discussion, and as pointed out by previous authors,[35] the inverted absorption spectrum observed in SEIRSE is not intrinsic to the optical enhancement effect but is associated with relative changes in the p- and s-polarized Fresnel factors of the four-phase multilayer system as a result of roughness-induced changes in the dielectric function of the Au film. Therefore, the maximum frequency and integrated area of the inverted peaks observed in Figures 3A and 4A (as well as those in Figures 3C and 4C) can be analyzed in the same way as one usually does to obtain vibrational peak frequencies and intensities from traditional IR absorption spectra.

Apart from the above-discussed peak inversion effect, another noticeable difference between the enhanced and unenhanced

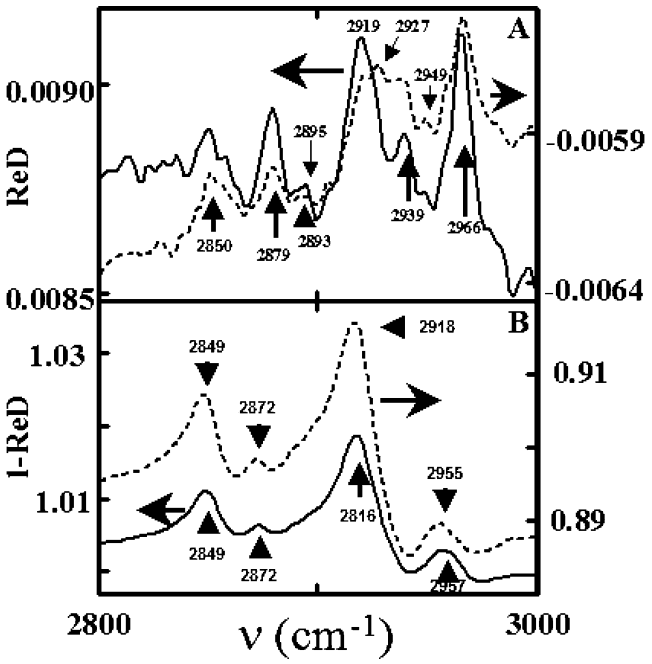

Figure 5. (A) Plots of Re*D* against wavenumbers for UDT (solid line, scale on the left) and DDT (dashed line, scale on the right), recorded using IRSE on a 188 nm thick gold film. (B) Plots of the quantity (1-Re*D*) for UDT (solid line, scale on the left) and DDT (dashed line, scale on the right) recorded using SEIRSE on a disordered, rough Au substrate. The Re*D* data for panel B are taken from the solid line plots of Figures 3A and 4A.

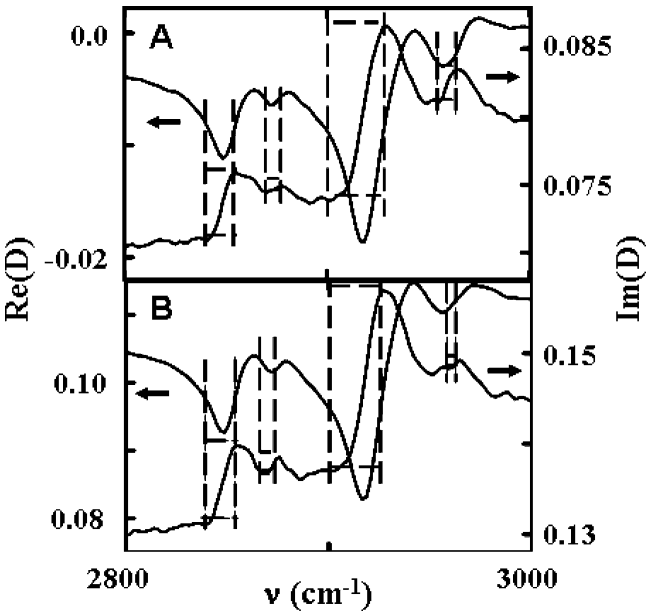

Figure 6. Schematic illustration of the procedure used to determine the empirical absorption strength *S* (defined in eq 5) using combined plots of Re*D* (data taken from Figures 3A and 4A) and Im*D* (data taken from Figures 3B and 4B). The SAMs used are UDT and DDT in A and B, respectively. The rectangular boxed areas associated with each absorption feature represent the un-normalized value [$\Delta\nu\Delta$(Im*D*)] of the absorption strength *S*. The boxed area (absorption strength) associated with the r_a^- mode ($\sim$2960 cm^{-1}) is smaller for the even-carbon DDT than for the odd-carbon UDT, and an opposite behavior is exhibited by the r^+ mode ($\sim$2975 cm^{-1}); this indicates how the presence of odd−even effect is detected in SEIRSE.

spectra in Figures 3 and 4 is the poor signal-to-noise ratio observed in the unenhanced Im*D* spectra (dashed lines in Figures 3B and 4B). The difficulties associated with the reliable measurement of Im*D* in the unenhanced spectra are clearly manifested in the weak spectral signature of this parameter. Because the thicknesses of the UDT and DDT films are similar, the change in phase between the bare and SAM-coated surfaces for the two molecules should be very similar. Thus, under ideal conditions, the values of Im*D* for the two cases should also have similar values. The data in Figures 3B and 4B, however, show comparable magnitudes but different signs of Im*D* for UDT and DDT. This implies that the experimental data for the unenhanced Im*D* are considerably affected by background noise and measurement uncertainties (most of which come from unavoidable variations in the probe beam and detector in different experimental runs). Thus, no useful information about the vibrational features of the SAMs could be obtained from these specific data, and this is indicated in the fourth column of Table 1. On the other hand, the enhanced Im*D* spectra (solid lines in Figures 3B and 4B) are well defined and clearly resolve all the necessary vibrational features of both SAMs (some of which are not even resolved in the enhanced Re*D* and A_p spectra). Thus, the phase information, which is embedded in the ellipsometric data but is difficult to extract with IRSE, is readily available from the Im*D* spectra obtained with SEIRSE. As we demonstrate in the following, these enhanced Im*D* spectra can be utilized for straightforward measurements of IR absorption peaks (widths and areas) that are superimposed on ill-defined baselines of background signals.

Measurement of Widths of IR Absorption Peaks Using SEIRSE. Widths of IR absorption peaks of a SAM formed on a solid substrate are frequently used as a measure of the structural order and surface density of the SAM.[36−40] Widths of such absorption peaks are also used to determine how surrounding solvents affect the homogeneity of SAM orientations.[41,42] Moreover, the width of the IR absorption peaks of a SAM represents an important parameter in the scalar optical response function often used for quantitative spectral analysis of SAMs.[43] Similarly, the integrated intensity under the IR absorption peak can be used as a signature feature of the order of adsorbed SAMs.[44] As we noted in the context of eq 1, the optical absorption peaks of the experimental SAM in IRSE are found in the Re*D* spectrum. Measurement of the widths and areas of such peaks usually requires a "baseline correction" to subtract the continuous background from the recorded spectrum, and this often becomes a nontrivial task if the experimental data do not indicate well-defined baselines. This difficulty of locating an appropriate baseline can be noted in both the unenhanced (dashed lines) and enhanced (solid lines) spectra of Re*D* (Figures 3A and 4A) and A_p (Figures 3C and 4C) recorded in our present work. The same problem is also encountered in FT-IRRAS as well as in polarization modulated Fourier transform infrared reflection absorption spectroscopy.[1] As we now explain below, the Im*D* spectra obtained with SEIRSE can be used to effectively address this specific problem of analyzing IR absorption peaks.

The spectra for Re*D* and Im*D* are correlated through the Kramers−Kronig relation. Thus, in SEIRSE, an approximately bell-shaped (inverted) feature of Re*D* gives rise to a dispersion-like behavior of Im*D* within the spectral region of each vibrational signature of the SAMs. The dispersion curve is nearly symmetric around the spectral position of the absorption band. Superposition of these two spectra can be used to identify fully resolved optical absorption peaks. This concept is demonstrated in Appendix A using simple considerations of the Drude−Lorentz model for optical absorption.

Figure 6 illustrates the use of Im*D* for the determination of absorber strengths of the key modes in the spectral region of

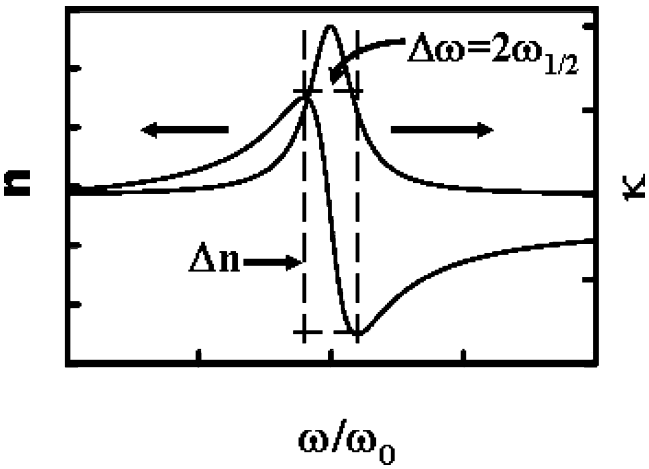

Figure 7. Schematic plots of κ and n (imaginary and real parts, respectively) for the complex index of a light absorbing material according to the Drude−Lorentz oscillator model described in eqs A.1 and A.2. Only a single absorption mode at a resonance frequency ω_o is considered. The X-axis represents the normalized frequency, ω/ω_o, of the oscillator. The two plots are appropriately scaled to be superimposed on each other. The rectangular area, drawn on the n plot, is defined by the difference between the maximum and minimum amplitude multiplied by the corresponding peak-to-peak width. In the limit of small dissipation, the extremum points of the n plot locate the fwhm frequencies on the corresponding κ graph.

CH_2/CH_3 stretching vibrations for UDT (panel A) and DDT (panel B). The ReD (scale on the left side of the graphs) and ImD (scale on the right side) are plotted together to identify singular absorption peaks among the observed vibrational features. Using this technique, we can resolve the in-plane and out-of-plane components of the convoluted CH_3 asymmetric stretching modes only hinted at by the slight downshift in peak location on ReD curves going from UDT to DDT. The rectangular areas shown in Figure 6 are constructed using the concept of absorption strength measurement illustrated in Figure 7. In this approach, the empirically defined spectral absorption strength S for the vibrational feature centered at wavenumber ν_0 is evaluated as

$$S(\nu_0) = C_0[\Delta\nu\Delta(\mathrm{Im}D)] \quad (3)$$

Here, C_0 is an empirical proportionality constant (in the unit of centimeters) that can be eliminated in the data analysis by normalizing S for each observed vibrational mode with respect to a standard absorption peak in the spectrum. $\Delta\nu$ (horizontal length of a given shaded box in Figure 6) is the fwhm of the given ReD feature, that is, the wavenumber separation between the extrema points of the corresponding dispersion in ImD. The results of this analysis, including fwhm and resonant frequencies taken from both the peak values of ReD and as the midpoint of the extrema widths from ImD, are tabulated in Table 1.

Odd−Even Effect of IR Absorption. As we noted earlier in this paper, comparison of the CH_3 symmetric (r^+) and asymmetric (r_a^-) mode intensities between the UDT and DDT SAMs should indicate if the odd−even effect of IR absorption is detected. Such a comparison cannot be reliably applied to the unenhanced ReD spectum in Figure 5A, because the absorption peaks there are superimposed on unknown baselines. The enhanced ReD data (Figures 3A, 4A, and 5B) are also not quite adequate for such analysis, because some of the weaker features are not entirely resolved in these plots. However, the ImD data combined with the ReD plots in Figure 6 indicate the presence of the odd−even effect. This is most visible in the raw data of ImD for the odd-carbon UDT, where the CH_3 symmetric (r^+) absorption is higher than the CH_3 asymmetric ip (r_a^-) absorption. We note in this context that the CH_2 stretch modes most probably enjoy a greater optical enhancement compared to that of the CH_3 modes, as a result of the closer proximity of the CH_2 molecules to the metal substrate. However, since the odd−even effect entails both increasing and decreasing absorption for modes experiencing the same environment, the fields should be essentially equivalent for the CH_3 stretch modes for both SAMs even with the slight difference in the surface-to-terminal methyl group distance between UDT and DDT.

TABLE 2: Optical Parameters Describing Odd−Even Effect in the ImD Data Obtained with SEIRSE

mode	SAM	wavenumber[a] (cm^{-1})	fwhm[b] (cm^{-1})	absorption strength, S[c]
CH_2 sym	UDT	2847	14	0.070
(d^+)	DDT	2849	16	0.140
CH_3 sym	UDT	2876	8	0.036
(r^+)	DDT	2874	7	0.015
CH_2 asym	UDT	2914	27	0.346
(d^-)	DDT	2914	24	0.459
CH_3 asym, ip (r_a^-)	UDT	2960	10	0.024
	DDT	2962	6	0.005
CH_3 asym, op (r_b^-)	UDT	2951	4	weak[d]
	DDT	2954	6	weak[d]

[a] Midpoint frequency between extremum points of plots in Figure 6. [b] Indicated by the horizontal lengths of shaded areas shown in Figure 6. [c] Defined in eq 3 and evaluated by taking $C_0 = 1$ cm. [d] Features are too weak to provide reliable values of S.

To eliminate possible contributions from different enhancement factors of the two substrates and the proximity effects, we focus on the internally normalized ratio of the CH_3 symmetric/asymmetric mode strengths sensitive to the odd−even effect, namely, $[S(r^+)]/[S(r_a^-)]$. Using the data presented in the last column of Table 2, we find that $[S(r^+)]/[S(r_a^-)]$ has the values of 1.5 and 3.0 for UDT and DDT, respectively. This 100% difference between the values of $[S(r^+)]/[S(r_a^-)]$ for the two molecules clearly indicates the presence of the odd−even effect discussed in the Introduction.

The above-mentioned internal normalization scheme used to determine $[S(r^+)]/[S(r_a^-)]$ can also be applied to the CH_2 modes to examine the absorption ratio parameter $[S(d^+)]/[S(d^-)]$ for the latter modes. In this case, however, the parameter $S(d^-)$ is associated with a relatively large experimental uncertainty because, as seen in Figure 6, accurate determination of the fwhm of the broad peak of ImD for the d^- mode is difficult; this Im$D(d^-)$ peak contains contributions from the unresolved (2935 cm^{-1}) adsorption band r_{FR}^+. Thus, using the largely uncertain values of $S(d^-)$, we obtain the values of $[S(d^+)]/[S(d^-)]$ to be 0.20 and 0.30 for UDT and DDT, respectively. According to the idealized model of all-trans CH_2 with equal tilt and rotation angles, $[S(d^+)]/[S(d^-)]$ should be the same for the two SAMs used. As expected, however, due to the uncertainties in the value of $S(d^-)$, we find a 50% difference between the values of $[S(d^+)]/[S(d^-)]$ for UDT and DDT.

It should be noted in the ImD data of Figure 5 that both the r^+ and r^- absorption bands are considerably better resolved than the d^- band. Thus, the values of $[S(r^+)]/[S(r_a^-)]$ determined here through internal normalization of absorption strengths are much more reliable than those of $[S(d^+)]/[S(d^-)]$ obtained by using the same procedure. In fact, if we take the observed 50% uncertainty in the value of $[S(d^+)]/[S(d^-)]$ as the maximum uncertainty for all measurements of the S-parameters considered here, then the observed 100% difference in the values of $[S(r^+)]/[S(r_a^-)]$ for UDT and DDT are still considerably above the level

of this very conservative estimate of uncertainty. In other words, the $[S(r^+)]/[S(r_a^-)]$ ratios measured here represent a definite effect where $S(r^+)$ increases and $S(r_a^-)$ simultaneously decreases as we go from UDT to DDT. This appears to be a definite manifestation of the odd−even effect, as anticipated in terms of intensity modulations for the all-trans adsorption configuration of the SAMs used.

5. Conclusions

The present work demonstrates the essential features of the technique of SEIRSE, which can serve as a useful vibrational spectroscopic tool for studying structural and electronic properties of SAMs on Au. Optical enhancement of IR absorption spectra has been studied previously with the utilization of localized surface plasmon resonance that occurs in rough surface structures of Au and Ag.[22,23,35] To our knowledge, however, the present report describes the first experimental study where the plasmon-induced surface-enhancement mechanism is incorporated in the framework of infrared ellipsometry. Using two model SAMs of comparable lengths, we have shown here how SEIRSE can distinguish between vibrational signatures of small changes in the terminal-methyl orientations of the two SAMs. This sensitivity of SEIRSE is demonstrated through the detection of the "odd−even" effect of IR absorption. In addition to optical absorption data, SEIRSE provides useful phase information in the form of the imaginary optical density function, Im*D*. This latter information is not available in traditional infrared reflection absorption spectroscopy and is considerably masked by background noise in unenhanced IRSE. The combination of the enhanced Im*D* and Re*D* spectra obtained with SEIRSE provides a phenomenological framework for determining widths and absorption strengths of IR spectral bands without having to guess the unknown baselines of these spectra. The spectroscopic sensitivity of this technique for probing molecular orientation is also associated with its capability for obtaining the optical phase data. With its further exploration, SEIRSE can be developed as a powerful probe of both overall (angle θ in Figure 1) and local (angles α and β in Figure 1) orientation effects of adsorbed SAMs on Au. Experiments addressing these specific aspects of SEIRSE are currently under way in our laboratory, and the results of these experiments will be presented in a future report.

Acknowledgment. This work was supported by the United States Department of Energy, the New York State Office of Science, Technology and Academic Research (NYSTAR), and by the National Science Foundation (Grant #INT-0206923).

Appendix A: Considerations for the Analysis of Spectral Absorption Strengths Using Re*D* and Im*D* Spectra

The empirical absorption strength, $S(\nu_0)$ (defined in eq 3), used for data analysis in our present work is based on the observation that the SEIRSE data for Re*D* and Im*D* closely resemble the imaginary (κ) and real (n) parts of the complex refractive index ($\hat{n}$) of an absorbing medium, respectively. To illustrate the basic underlying concept that allows us to introduce the parameter $S(\nu_0)$, let us use the simple Drude−Lorentz model of the refractive index ($\hat{n} = n + j\kappa$)of an optically absorbing material. In the limit of small damping ($\gamma \ll \omega_0$), the n and κ (for a single oscillator) have the following simple forms according to the standard Drude−Lorentz formulation,[1,39]

$$n = 1 + \frac{Nq^2}{2m\epsilon_0 c}\left[\frac{{\omega_0}^2 - \omega^2}{({\omega_0}^2 - \omega^2)^2 + \gamma^2\omega^2}\right] \quad \text{(A.1)}$$

$$\kappa = \frac{Nq^2}{2m\epsilon_0 c}\left[\frac{\omega^2\gamma}{({\omega_0}^2 - \omega^2)^2 + \gamma^2\omega^2}\right] \quad \text{(A.2)}$$

where N is the number of oscillators, q the charge on the oscillator, m their mass, ϵ_0 the permeability of free space, c the speed of light, γ the damping constant, and ω_0 the circular resonance frequency ($\omega_0 = 2\pi\nu_0$), where ν_0 is the linear resonance frequency. The functions defined in eqs A.1 and A.2 are schematically plotted in Figure 7. The integrated area under the Lorentzian plot of κ represents a measure of the strength of the optical absorption. The fwhm of this curve is equal to $\Delta\omega = \omega_{+1/2} - \omega_{-1/2}$ where $\omega_{\pm 1/2}$ represents the half-maximum frequencies: $\omega_{\pm 1/2} = \omega_0 \pm (\gamma/2)$. At these half-peak frequencies, $n(\omega_{\pm 1/2}) = 1 \pm [(Nq^2)/(4\epsilon_0 m\omega_0\,\gamma)]$, where the upper and lower signs correspond to the maximum and minimum values of n around the absorption peak. Thus, the extremum points in the plot of n locate the half-maximum frequencies of κ, which is the Kramers−Kronig transform of n. The product of the difference ($\Delta n = Nq^2/[2\epsilon_0 m\omega_0\,\gamma)$]) in the extrema of n with the fwhm ($\Delta\omega = \gamma$) is independent of the dissipation constant in the limit, $\gamma \ll \omega_0$. As noted in Figure 6 by the rectangular boxed area, the quantity ($\Delta n\Delta\omega$) is also proportional to the integrated area under the plot of κ and, hence, for the purpose of simple data analysis can be taken as an empirical measure of the strength of optical absorption. This very concept can be extended to the analysis of the surface-enhanced Re*D* and Im*D* spectra. Im*D* in SEIRSE displays the characteristic shape of n and, when superimposed on Re*D*, should efficiently resolve resonant modes giving an adequate measure for the strength of optical absorption located within the half-maximum frequencies. This eliminates the need for determining a baseline for peak-width analysis in SEIRSE.

References and Notes

(1) Roy, D.; Fendler, J. H. *Adv. Mater.* **2004**, *16*, 479.
(2) Drevillon, B. *Thin Solid Films* **1998**, *313−314*, 625.
(3) Tiwald, T. E.; Thompson, D. W.; Woollam, J. A.; Paulson, W.; Hance, R. *Thin Solid Films* **1998**, *313−314*, 661.
(4) Tiwald, T. E.; Woollam, J. A.; Zollner, S.; Christiansen, J.; Gregory, R. B.; Wetteroth, T.; Wilson, S. R. *Phys. Rev. B* **1999**, *60*, 11464.
(5) Kasic, A.; Schubert, M.; Einfeldt, S.; Hommel, D.; Tiwald, T. E. *Phys. Rev. B* **2001**, *62*, 7365.
(6) Garcia-Caurel, E.; Drevillon, B.; De Martino, A.; Schwartz, L. *Appl. Opt.* **2002**, *41*, 7339.
(7) Tiwald, T. E.; Thompson, D. W.; Woollam, J. A.; Paulson, W.; Hance, R. *Thin Solid Films* **1998**, *313−314*, 661.
(8) Bradford, D. C.; Hutter, E.; Assiongbon, K. A.; Fendler, J. H.; Roy, D. *J. Phys. Chem. B* **2004**, *108*, 17523
(9) Osawa, M. *Bull. Chem. Soc. Jpn.* **1997**, *70*, 2861.
(10) Osawa, M. Surface-Enhanced Infrared Absorption. In *Near-Field Optics and Surface Plasmon Polaritons*; Kawata, S., Ed.; Springer-Verlag: Berlin, Germany, 2001; Vol. 81, p 163.
(11) Jensen, T. R.; Van Duyne, R. P.; Johnson, S. A.; Maroni, V. A. *Appl. Spectrosc.* **2000**, *54*, 371.
(12) Goutev, N.; Futamata, M. *Appl. Spectrosc.* **2003**, *57*, 506.
(13) Laibinis, P. E.; Whitesides, G. M.; Allara, D. L.; Tao, Y.-T.; Parikh, A. N.; Nuzzo, R. G. *J. Am. Chem. Soc.* **1991**, *113*, 7152.
(14) Ulman, A. *Chem. Rev.* **1996**, *96*, 1533.
(15) Roy, D. *Opt. Commun.* **2001**, *200*, 119.
(16) Dignam, M. J.; Moskovits, M.; Stobie, R. W. *Trans. Faraday Soc.* **1971**, *67*, 3306.
(17) Korte, E.-H.; Röseler. A. *J. Mol. Struct.* **2003**, *661−662*, 579−585.
(18) Dluhy, R. A.; Stephens, S. M.; Widayati, S.; Williams, A. D. *Spectrochim. Acta* **1995**, *51*, 1413.
(19) Meuse, C. W. *Langmuir* **2000**, *16*, 9483−9487.

(20) Hutter, E.; Assiongbon, K. A.; Fendler, J. H.; Roy, D. *J. Phys. Chem. B* **2003**, *107*, 7812.
(21) Axelsen, P. H.; Citra, M. *J. Prog. Biophys. Mol. Biol.* **1996**, *66*, 227.
(22) Parikh, A. N.; Allara, D. L. *J. Chem. Phys.* **1992**, *96*, 927.
(23) Osawa, M.; Ataka, K.-I. *Surf. Sci. Lett.* **1992**, *262*, L118.
(24) Love, J. C.; Estroff, L. A.; Kriebel, J. K.; Nuzzo, R. G.; Whitesides, G. M. *Chem. Rev.* **2005**, *105*, 1103.
(25) Nishi, N.; Hobara, D.; Yamamoto, M.; Kakiuchi, T. *J. Chem. Phys.* **2003**, *118*, 1904.
(26) Gupta, V. K.; Abbott, N. L. *Langmuir* **1999**, *15*, 7213.
(27) Nuzzo, R. G.; Korenic, E. M.; Dubois, L. H. *J. Chem. Phys.* **1990**, *93*, 767.
(28) Hutter, E.; Fendler, J. H.; Roy, D. *J. Phys. Chem. B* **2001**, *105*, 11159.
(29) He, L.; Shi, Z. Q. *Solid-State Electron.* **1996**, *39*, 1811.
(30) Liu, Z. H.; Brown, N. M. D. *Thin Solid Films* **1997**, *300*, 84.
(31) Stobinski, L.; Zommer, L.; Dus, R. *Appl. Surf. Sci.* **1999**, *141*, 319.
(32) Snyder, R. G.; Marconcelli, M.; Strauss, H. L.; Hallmark, V. M., *J. Phys. Chem.* **1986**, *90*, 5623.
(33) Mielczarski, J. A.; Yoon, R. H. *J. Phys. Chem.* **1989**, *93*, 2034.
(34) Golden, W. G.; Saperstein, D. D.; Severson, M. W.; Overend, J. *J. Phys. Chem.* **1984**, *88*, 574.
(35) Nishikawa, Y.; Fujiwara, K.; Ataka, K.-I.; Osawa, M. *Anal. Chem.* **1993**, *65*, 556.
(36) Hatzor, A.; Moav, T.; Cohen, H.; Matlis, S.; Libman, J.; Vaskevich, A.; Shanzer, A.; Rubinstein, I. *J. Am. Chem. Soc.* **1998**, *120*, 13469.
(37) Vanderah, D. J.; Parr, T.; Silin, V.; Meuse, C. W.; Gates, R. S.; La, H.; Valincius, G. *Langmuir* **2004**, *20*, 1311.
(38) Engquist, I.; Liedberg, B. *J. Phys. Chem.* **1996**, *100*, 20089.
(39) Harrick, N. J. *Internal Reflection Spectroscopy*; Harrick Scientific Corp.: Ossining, NY, 1979.
(40) Vallant, T.; Brunner, H.; Mayer, U.; Hoffmann, H.; Leitner, T.; Resch, R.; Friedbacher, G. *J. Phys. Chem. B* **1998**, *102*, 7190.
(41) Yan, D.; Saunders, J. A.; Jennings, G. K. *Langmuir* **2003**, *19*, 9290.
(42) Harder, P.; Grunze, M.; Dahint, R.; Whitesides, G. M.; Laibinis, P. E. *J. Phys. Chem. B* **1998**, *10*, 426.
(43) Kang, J. F.; Kurth, D. G.; Ulman, A.; Jordan, R. *Langmuir* **1999**, *15*, 5555.
(44) Bensebaa, F.; Voicu, R.; Huron, L.; Ellis, T. H.; Kruus, E. *Langmuir* **1997**, *13*, 5335.